

Shock-Wave Boundary-Layer Interaction Study on a Compression Corner Using Pressure-Sensitive Paint

C. Manisankar, S. B. Verma and C. Raju

Scientists, Council of Scientific and Industrial Research, National Aerospace Laboratories (NAL), Experimental Aerodynamics Division, Bangalore - 560017, INDIA

Abstract

Experiments have been performed to study a compression corner induced turbulent boundary layer interactions in a freestream Mach number of 2.05 without and with control. Two configurations of vortex generators (VG), in the form of an array of delta-ramps placed upstream of the interaction region at 27.5δ or $h/\delta = 0.65$, have been tested to control the interaction. Pressure sensitive paint (PSP) measurements were made using a binary paint developed in-house. Reasonably good agreement of PSP results with mean static pressure measurements has been observed. The spanwise wall pressure distribution immediately downstream of the control devices show a sinusoidal pattern indicating the generation of streamwise vortices from VG devices. The interaction of these vortices with the reverse flow in the separated region replaced a well-defined separation line for no control by a highly corrugated separation line. Relative to the no-control case, the peak *rms* value in the intermittent region of separation with control showed significant modifications based on each VG configuration suggesting the effectiveness of VG devices in controlling the amplitude of shock oscillations in such interactions.

NOMENCLATURE

h	Maximum height of the VG ramp, mm
δ	Boundary-layer thickness, mm
f_s	Characteristic frequency of shock motion, Hz
$G(f)$	Power spectral density, (psi ² /Hz)
L_s	Length of separation, mm
M_∞	Freestream Mach number
P_0	Pressure in the stagnation chamber of the wind tunnel, psia
P_∞	Freestream static pressure, psia
P_w	Local wall pressure, psia
s	Spacing in the vertex of the vortex generating delta ramps, mm
σ/P_w	Non-dimensionalized local <i>rms</i> of wall pressure
T_0	Stagnation temperature, K
U_∞	Freestream velocity, ms ⁻¹

1. INTRODUCTION

Shock-wave boundary-layer interactions (SWBLI) are indispensable in both internal and external supersonic flows and can cause separation of the incoming boundary-layer. The process of separation is generally associated with low-frequency oscillations of the separation shock (e.g., with Strouhal number ($St = f_s L_s / U_\infty$) for compression ramp flows between 0.02–0.05 [3–4, 6]) and often leads to) increased aerodynamic drag, heat transfer and fluctuating pressure loads [1–3]. Much of these early studies were however focused on understanding the dynamic/unsteady behavior of these interactions [2] and identifying its causes [4–6].

Recently, studies have been carried out to diminish the detrimental effects of SWBLI using flow control devices [7–10]. These techniques primarily rely on altering the characteristics of the incoming

boundary-layer by adding momentum to the velocity profile close to the wall [7] by the use of vortex generating (VG) devices such as micro-ramps, vane-type VGs or micro-jets at an appropriate distance upstream of the region of interaction [7–10]. The aim is to reduce the shock strength and hence, reduce the extent of separation with the aim of reducing shock unsteadiness or both [11]. Recent studies [7, 10, 12–13] have also revealed that sub-boundary-layer control devices (i.e., with h/δ of 0.1 – 0.4) are more effective in stabilizing the interaction region relative to conventional vane-type VG devices. However, the choice of VG placement location depends primarily on the type of interaction and the flow Mach number [8]. The major flow diagnostics used in all the previous studies were primarily discrete surface pressure measurements, surface oil flow and schlieren visualization.

The main objective of the present investigation is to study the effectiveness of control devices in controlling the interaction induced by a compression ramp. For this purpose, PSP technique has been used as it is a useful tool that provides global imaging as well as quantitative data. Additionally, real-time pressure data using Kulite sensors has also been acquired. Investigations were conducted on a 24 deg compression corner to control the overall separation characteristics using mechanical VG devices at a freestream Mach number of 2.05. Two different VG configurations were implemented in separate tests upstream of the interaction region at 27.5δ . The interaction is studied using fast piezo-resistive Kulite pressure sensors, surface oil-flow and schlieren visualization.

2. EXPERIMENTAL SET UP AND PROCEDURE

2.1. Wind tunnel facility and model details

Tests were conducted in the 0.457 m \times 0.3 m blow-down tri-sonic wind-tunnel of the Experimental Aerodynamics Division at National Aerospace Laboratories (NAL). The compression corner model was mounted on a sting along the tunnel centerline in order to avoid effects of noise levels from turbulent boundary-layer present on wind-tunnel wall. In the present experiments, the test Mach number was 2.05 ± 0.02 (freestream velocity, $U_\infty = 523 \text{ ms}^{-1}$) while the stagnation pressure (P_0) and temperature (T_0) was $208.5 \text{ kPa} \pm 2\%$ (absolute) and $298 \text{ K} \pm 0.4\%$, respectively. This resulted in a unit Reynolds number (Re/L) of $25.257 \times 10^6 \text{ m}^{-1}$. The wall temperature was approximately adiabatic. The flat-plate of the model was 28 cms long with a span of 11 cms, Fig. 1 (a), and the ramp angle was fixed at 24 degrees.

The Reynolds number based on the flat-plate length was 7.072×10^6 . No side-fences were used in order to facilitate schlieren imaging. A boundary-layer trip, made of 60 grit carborundum particles spanning 4 mm in length and placed at 17 mm from the leading edge, was used to ensure sufficiently

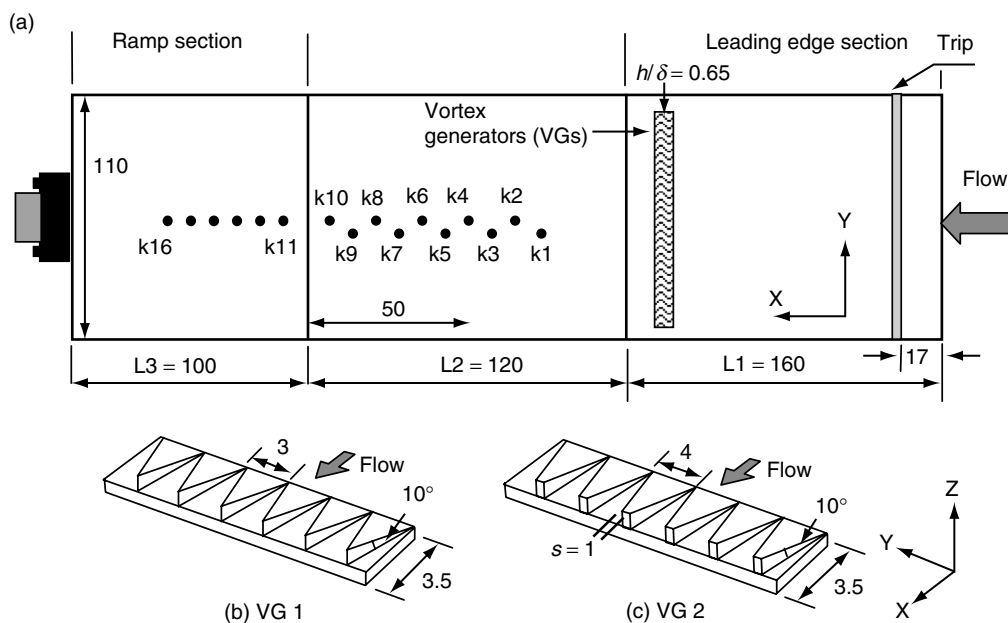


Figure 1. Schematic showing (a) The compression corner model details with the sensor locations and the two locations at which VG devices are tested, (b)-(c) The two VG configurations used in the present study. All dimensions are in mm.

thick (turbulent) boundary-layer so that the control devices are well embedded in them. The boundary-layer thickness was estimated based on length Reynolds number Re_x for turbulent flows and then corrected for compressible flows as per the procedure suggested by Van Driest [15–16] for Mach number greater than unity. It may however be noted that such an estimation may differ from the boundary-layer thickness calculated from velocity profile by $\pm 3\%$ [17]. Further, assuming that transition occurs at about 1.1×10^6 [18], the length Reynolds number of 4.04×10^6 , about 120 mm upstream of the compression corner, suggests that the boundary-layer to be fully developed.

Control devices in the form of an array of single-row delta ramps were used to modify the flow interaction, as shown in Figs. 1 (b) and (c). These configurations were initially chosen to investigate the effect of spanwise spacing ‘ s ’ of the vertex of the ramps [13] in controlling the amplitude of shock unsteadiness in the intermittent region of separation. The VG devices were introduced upstream of the interaction and tested for a streamwise location of 130 mm upstream of the corner, as shown in Figs. 1 (a). With respect to the interaction location (approx. 20 mm upstream of corner where $\delta = 4.0$ mm), this location corresponds to 27.5δ , whereas with respect to the height ‘ h ’ of the delta-ramps, this corresponds to h/δ of 0.65, respectively.

2.2. PSP sensor and instrumentation

The PSP measurements were conducted in the solid-wall test section of the tunnel with the optical access provided by the modified sidewall-mounted Schlieren window, Fig. 2. The compression corner surfaces and a calibration sheet (a thin aluminium sheet of size 200 mm \times 300 mm) were spray coated with a pyrene based binary PSP (NAL-G8), developed in-house. A few coupons (30 mm \times 25 mm) were cut from the calibration sheet and calibrated in an external calibration chamber, where an environment with controlled pressure and temperature was created. Table 1 shows the photo-physical properties of the NAL G-8 paint. Figure 3 (a) shows the calibration curve of NAL-G8 and the calibration coefficients obtained from the coupons were later utilized for processing PSP images. The solid red line shows the polynomial fit. The dispersion of pressure sensitivity over the calibration coupon was observed to be less than 1% of the mean value. Figure 3 (b) shows the compression corner model, coated with PSP and with marker points for image registration, mounted in the 0.3 m tunnel.

The PSP system, Fig. 2, consisted of a ultra-violet (UV) flash lamp, two scientific-grade charge-coupled device (CCD) cameras, the calibration equipment, and an image-processing software package.

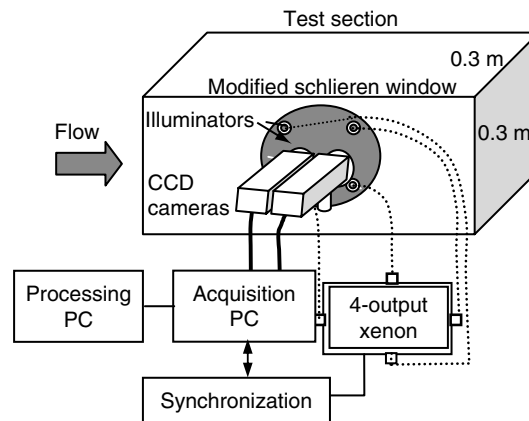


Figure 2. Schematic of the PSP set up in the 0.3 m wind tunnel. EAD.

Table 1. NAL G-8S PSP specifications

Excitation wavelength	330 (± 20) nm
Pressure sensitive emission (blue)	450–550 nm
Intensity sensitive emission (red)	600–650 nm (excitation reference)
Temperature sensitivity	0.1 to 0.2% / $^{\circ}$ C
Pressure sensitivity	66% bar at 25 $^{\circ}$ C (nominal)

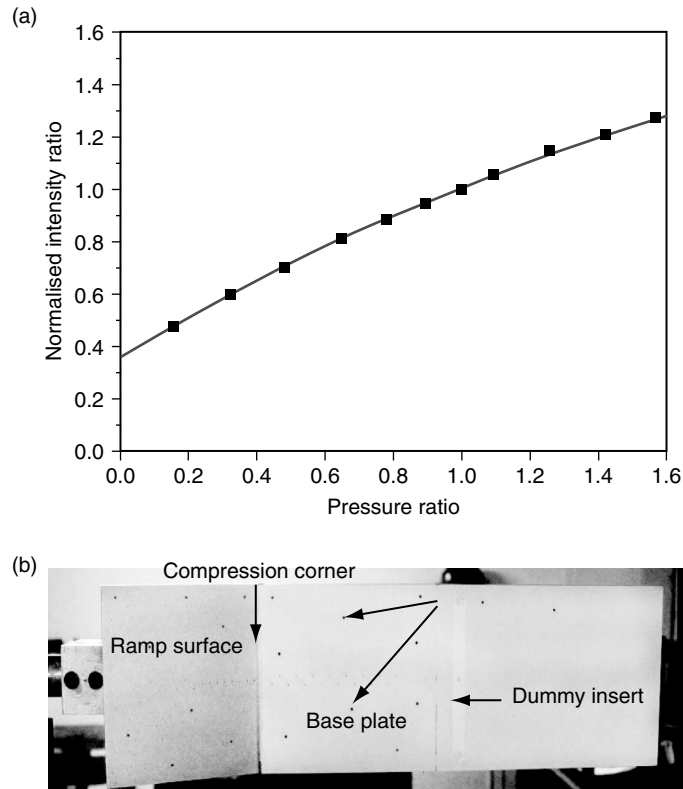


Figure 3. (a) Calibration curve for NAL-G8 paint and, (b) Photograph showing the compression corner model coated with PSP and with marker points mounted in the 0.3 m wind tunnel.

Excitation of the PSP on the model was provided by a xenon flash lamp system (OMT-D40-XE), with four light guides attached to four UV antireflection-coated quartz optics each consisting of collector and objective lenses emitting in the range of 330 (± 20) nm. The lamp could be triggered externally up to 35 Hz, with single pulse duration of 20 μ s. Optimum distribution of illumination on the entire model surface was obtained using four rotatable illuminator heads connected to the lamp system by four 15-m-long optical fiber cables. The paint emission data were acquired by two air-cooled scientific-grade 12-bit CCD slow scan cameras with resolution of 1280 \times 1024 pixels. A pressure sensitive image in the band of 450–550 nm and an excitation reference image in the band of 600–650 nm were acquired using blue and red transparent filter sets, respectively, supplied by the M/s Optische Messtechnik (OMT) GmbH, Germany. An objective of focal length 50 mm was utilized in each of the cameras to provide maximum spatial resolution of PSP images. The acquired intensity images were converted into pressure images using an image processing procedure using OMS processing software.

Two separate cameras were used to measure the two components of the binary sensor (the pressure sensitive component and the intensity sensitive or reference component). The image integration time was about 9 seconds (at flash frequency of 20 Hz), so as to have a large pixel fill ratio in the CCD array (to have large signal to noise ratio). Therefore, in the blow-down duration of about 20 seconds, only one set of images was acquired after allowing sufficient time for flow stabilization. The sequence of measurement involved acquisition of images from the two cameras (the pressure sensitive and the intensity sensitive) under different conditions: a) dark images b) pre-run/wind-off images c) wind-on images and d) post-run wind-off images. The potential sources of error introduced are through the process of converting the intensity images to pressure images which involves a series of steps that includes inputs from calibration, image alignment, ratioing, filtering, and finally mapping to the model geometric coordinates [14]. Since the test model was a flat plate, the image registration based on 20 image registration or marker points using a third degree polynomial fit was adequate [14]. The image misalignment was typically in the order of 1–2 pixels. The PSP data was averaged by applying a 5 pixel by 5 pixel median filter. Further in studies using binary PSP, where the two emissions from pressure sensitive and reference molecules are captured using two CCD cameras with separate filters, the angle

between the cameras contribute to errors apart from model movements. While the former has been taken care of in the PSP software, extra care was taken to ensure the model mounting on the tunnel walls was sturdy so that the model deflection was negligible.

Simultaneous wall pressure measurements along the centerline were made using fast piezo-resistive transducers (models XT-140M and XCQ-093). According to the manufacturer's specifications, these transducers have a natural frequency of approximately 250 kHz. The sensitivity of the transducers is typically 3–4 mV/psi. These transducers were calibrated statically. Nine such transducers were mounted upstream of the corner with a pitch of 5.5 mm while six of them were mounted on the ramp surface (with a pitch of 5 mm), Fig. 1. The transducer data was acquired using National Instruments truly simultaneous acquisition card NI4495 DC series (with 24-bit resolution) at a sampling frequency of 50 kHz. Each sensor was powered by a DC power supply, and the signal was passed through an amplifier and a signal conditioner. A low-pass filter of 20 kHz was applied during data processing. For each transducer channel, 200 records of 4096 were acquired yielding a total of 819, 200 data points per channel per tunnel run. For spectral analysis, a 4096-point narrowband Fast Fourier Transforms (FFTs) was performed and later averaged for 200 records, giving a frequency resolution of 12.2 Hz. The *rms* noise was found to be approximately one-fifth of the *rms* level beneath the Mach 2 boundary-layer. Both mean pressure and *rms* data was also extracted from each transducer signal.

Color schlieren technique (using a banded RGB filter at the knife-edge location upstream of the camera) has been used to capture the flow-field interaction using Palflash 501 light source with spark duration of 750 ns and pulse energy of 6 Joules. Schlieren images were captured using Nikon 1X digital camera with a 300 mm lens. The exposure time was set at 125 μ s.

3. RESULTS AND DISCUSSIONS

Figure 4 and 5 show color schlieren images and surface oil pictures of the interaction without and with VG2, respectively. The interaction region is characterized by λ -shock pattern consisting of separation and reattachment shocks that merge to form an interaction point (I, marked with a dashed circle) above the ramp section. Relative to the case without control, Fig. 4 (a), VG devices are seen to generate flow

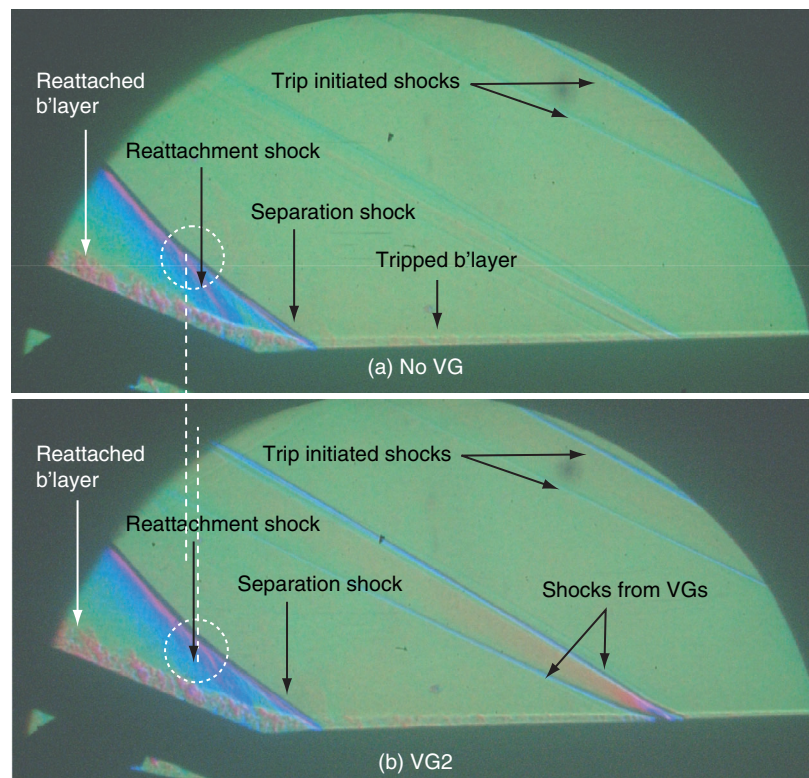


Figure 4. Color schlieren images of the flow over a 24° compression ramp for (a) no control (b) with VG2; $M_\infty = 2.0$ and $h/\delta = 0.65$.

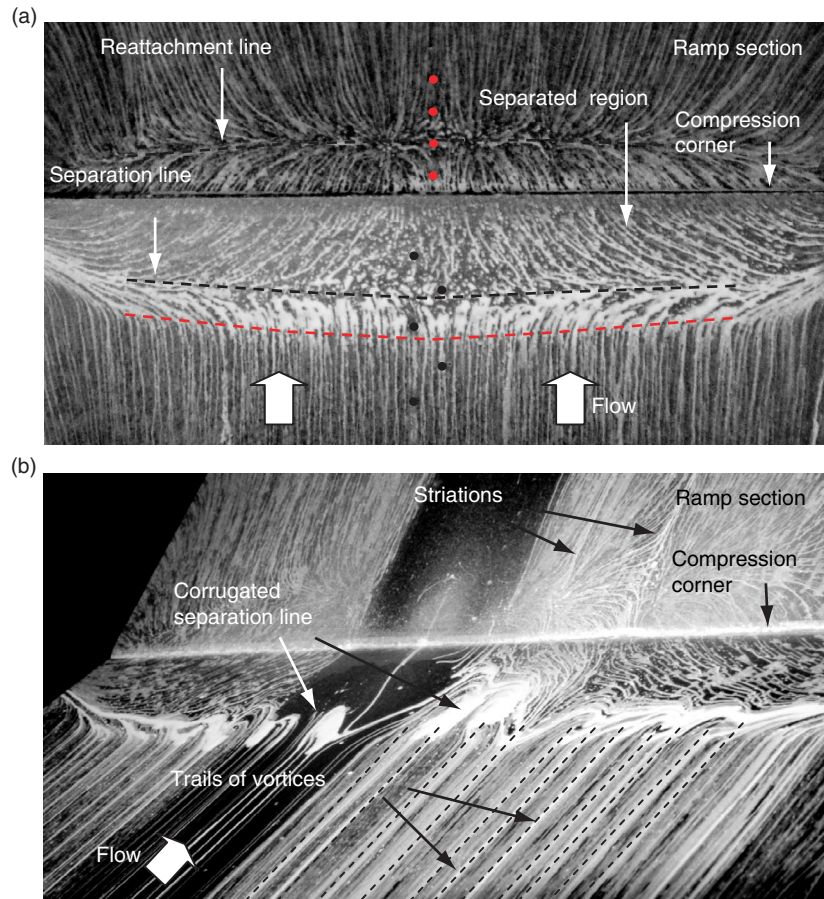


Figure 5. Comparison of surface flow pattern for (a) no control, (b) with VG2, showing the corrugated separation line and the trails of vortices.

perturbations - compression wave (inclined at 30° to the main flow and is the Mach angle for $M = 2$ flow) and expansion waves - locally. Also the reattaching boundary-layer is clearly seen to be relatively thicker with control.

A comparison of the surface oil pictures indicates significant modifications in the overall surface flow pattern without and with control. The picture in 5 (a) is taken from top, looking down on the plate. The flow direction is from bottom to top as shown by two white arrows. However, in Fig. 5 (b) the model picture was taken with the camera looking on the model from top right of the tunnel wall. The flow direction in this picture is from bottom left to top right. A well defined separation line, for the case of no control (Fig. 5 (a)), is seen to get replaced by a highly corrugated separation line with control (Fig. b (b)). Upstream of the interaction, traces of counter-rotating vortex pairs (CVP) are clearly indicated by trails of streamwise accumulation of oil pigment, Fig. 5 (b). The corrugations in the separation line are formed as a result of the interaction between the streamwise CVP and the reverse flow in the separated region [13]. A well defined reattachment line for no control case is also seen to be completely replaced by a striation pattern (beginning from ramp corner itself) with each striation originating exactly in line with the location of each crest of the corrugated separation line. Since these striations were not observed for the no control case, the origin of these is not due to the presence of Goertler vortices associated with reattaching boundary-layers but is clearly linked to the flow changes induced by the dramatic modification of the separation line.

Figure 6 (a) and (b) shows quantitative PSP pressure maps of the interaction for cases of without and with control (VG2). These pressure maps are obtained using an appropriate spatial filter (10 pixel \times 10 pixel Gaussian filter) to smoothen the PSP data [14]. The flow is from right to left and the dark regions on the image represent lower pressures and *vice-versa*. PSP data for the no control test case was

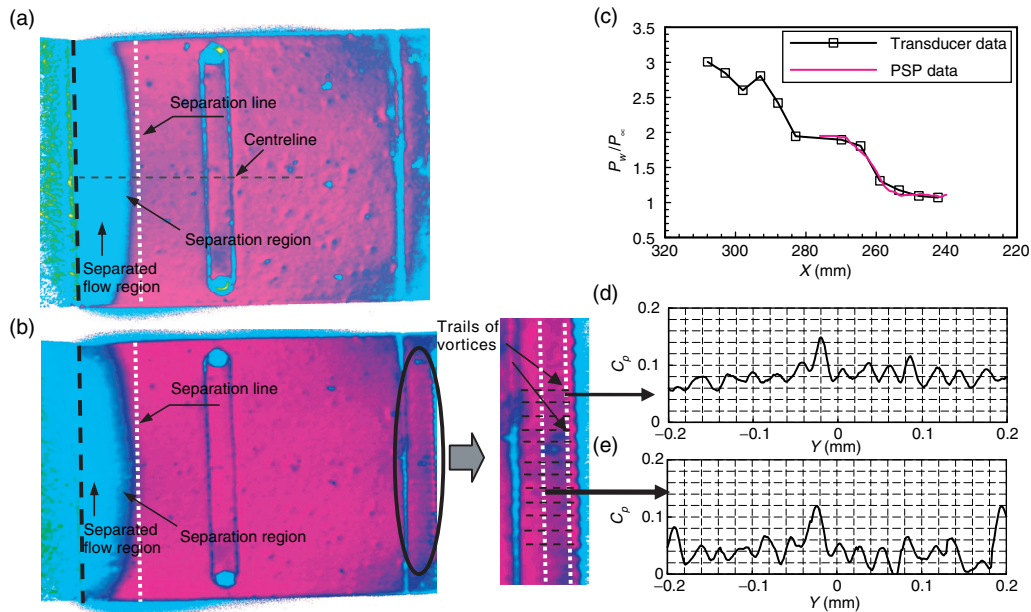


Figure 6. Quantitative PSP pressure maps of surface pressure (C_p) for (a) no VG, (b) with VG2 for $h/\delta = 0.65$ and, (c) comparison of the streamwise mean pressure distribution for no VG case from PSP and transducer measurements and (d)-(e) Spanwise variation in C_p for VG2 indicating trails of streamwise vortices.

extracted along the centerline, as shown by dashed line in Fig. 6 (a). It is seen that the comparison between the pressure port data and PSP for no control case, Fig. 6 (c), is generally good and the agreement in P/P_∞ is within ± 0.03 to 0.05 for most data.

In Figs. 6 (a) and (b), the region of interaction can be clearly seen on the flat plate but not on the ramp surface. The latter is due to the fact that the silica-gel particles in the compressed air supply constantly bombard the ramp surface as a result of which the paint gets contaminated with these particles. In fact after some runs, the PSP from the ramp surface is completely blown off due to the effect of these particles similar to sand blasting on a surface. Relative to the no VG case, a slight corrugation in the separation line can be observed for VG2 case but is not very prominent, as seen in oil pictures, Figs. 5 (b). However, the region of separation (seen as the dark blue region at the beginning of interaction and before the separated flow region) is observed to be much wider with control relative to no control case. This region seems to represent the streamwise extent of the corrugations, as seen in the oil pictures of Fig. 5.

Immediately downstream of the VG insert, trails of counter-rotating vortices can be observed (as shown by dashed lines on the zoomed portion) for over a short distance after which these trails disappear, Fig. 6 (b). This could be due to the fact that at this control device location, $h/\delta = 0.65$, the boundary-layer being thinner, the higher momentum air from the main flow is able to penetrate closer to the wall surface causing sufficient pressure changes to appear. Later on, as the vortices grow and interact with each other, these pressure changes reduce and so trails of vortices could not be seen any further in PSP pressure maps. Figure 6 (d) and (e) shows spanwise variation in C_p over these trails of vortices for two axial locations. The spanwise wall pressure variation shows a sinusoidal pattern indicating that the VG configurations successfully generate streamwise vortices that help modify the separation characteristics in the intermittent region of separation, observed earlier. Further downstream, however, these vortex trails could not be captured with PSP.

Figure 7 (a) shows a comparison of streamwise mean pressure distribution and its corresponding rms values for no control and with control [13]. Although no apparent change in the separation length is evident, however, the corresponding rms distributions show a significant reduction in peak rms value (of 50%) for VG1 in the intermittent region of separation, Fig. 7 (b). The VG2 configuration, however, shows a slight increase in this value. The characteristic frequency, f_s , of shock motion lies for the

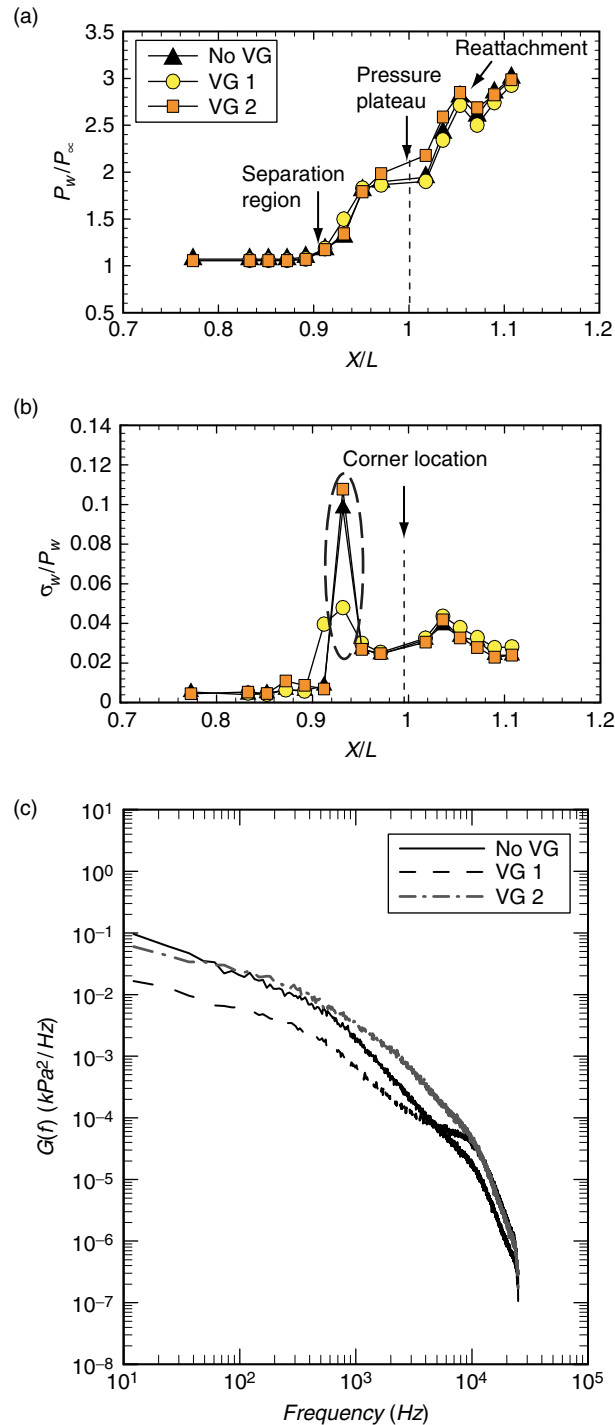


Figure 7. (a)-(b) Streamwise distribution of mean wall pressure and the corresponding rms values (c) Spectral plot of the fluctuating pressure signal in the intermittent region of separation (marked by long dashed ellipse) for the three test cases.

present case lies between 500 Hz–1300 Hz or $0.004 U_\infty/\delta$ to $0.01 U_\infty/\delta$ [13]. These high-amplitude low-frequency fluctuations attribute to the back-and-forth unsteady motion of the separation shock over the sensor location [13]. Spectral analysis of the pressure signal in the intermittent separation location shows dominance of relatively low-frequency, high-amplitude pressure fluctuations of the separation shock with no evidence of coherent shock-motion frequencies, Fig. 7 (c). Relative to the reference case, the amplitude of pressure fluctuations in the intermittent separation location, with VG2, is seen to

increase in the entire range. With VG1, on the other hand, a considerable drop in energy levels in compliance with *rms* values is observed [13]. It can be further observed that the presence of VG devices does not seem to alter the shock oscillating frequency but helps to reduce the amplitude of these frequencies (as is also seen from the *rms* plots, Figs. 7 (b)).

Figure 8 (a) shows one of the quantitative PSP pressure map of the interaction before the PSP coating on the ramp surface was blown away by the silica gel particles. It can be seen that in addition to the separation line on the base plate, the PSP pressure map also shows some indication of the striation flow pattern on the ramp surface (indicated by dashed lines), as was observed in surface oil flow pictures. However, useful quantitative pressure plots could not be extracted from the flow on the ramp surface due to reasons explained earlier.

Figure 8 (b) shows a comparison of the streamwise mean pressure distribution extracted from PSP measurements without and with control. Although no significant changes in the location of separation can be observed without and with control, the strength of separation shock for VG1 configuration is seen to be slightly reduced relative to no control case while that for VG2 configuration is relatively increased. Similar results were reported in ref. [13] using Kulite pressure transducers. Further detailed measurements are however needed to corroborate the variation in flow physics from each configuration for the present test conditions.

The above observations indicates that although PSP measurements were able to give a global pressure map of the interaction and reveal certain modified regions of interaction such as the region of separation or streamwise extent of corrugations, it was unable to detect small variations in wall pressure to reveal the traces of counter-rotating vortices up to the interaction and their consequent interaction with the flow in the region of interaction. To reveal detailed flow features in such flow control studies, it would be beneficial to (i) to increase the scale of the interaction such as by conducting the experiments on the tunnel wall with thicker boundary-layer and using larger VG configurations and,

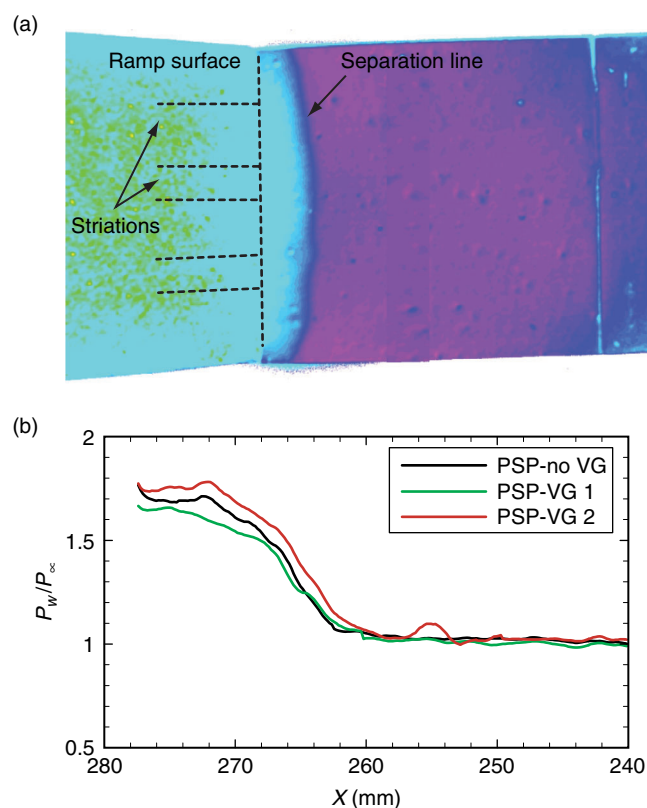


Figure 8. (a) Quantitative PSP pressure map of surface pressure (C_p) showing the flow pattern on the ramp surface for VG2 case and, (b) Comparison of the streamwise mean pressure distributions extracted from the surface pressure maps using PSP.

(ii) to conduct the paint calibration with much smaller pressure variations. Keeping these points in mind, future tests using PSP will be conducted accordingly.

ACKNOWLEDGEMENTS

The authors wish to thank the Aeronautical Research and Development Board (AR&DB) of India for supporting this project and Mr.Sathayanarayan, Scientist EAD for his support during execution of PSP measurements. The technical support of Mr. Perinaygam, Mr. Janardhan and Mr. Muthuswamy, staff of the 0.3 m wind tunnel facility at NAL during the test campaigns, is gratefully acknowledged.

4. CONCLUSIONS

An experimental study was conducted to study a compression corner induced turbulent-shock boundary layer interaction without and with control at a freestream Mach number of 2.05. Comparisons of the PSP results with conventional static pressure port measurements have shown generally excellent agreement along the symmetry plane. The spanwise wall pressure variation immediately downstream of the control devices shows a sinusoidal pattern indicating that the VG configurations successfully generate streamwise vortices that help modify the separation characteristics in the intermittent region of separation. Although no significant change in the separation length is evident from mean pressure transducer data, however, the corresponding *rms* distributions show a significant reduction in peak *rms* value (of 50%) for VG1 in the intermittent region of separation. The VG2 configuration, however, shows a 12% increase in this value. This indicates that the VG configuration with the sharpest delta ramp vertex gives the most favorable results and helps to alleviate the fluctuations of the separation shock and hence, the fluctuating pressure loads in the intermittent region of separation.

REFERENCES

- [1] Dolling, D.S. and Murphy, M.T., "Unsteadiness of the Separation Shock Wave Structure in a Supersonic Compression Ramp Flowfield," *AIAA Journal*, Vol. 21, No. 12, 1983, pp. 1628–1634.
- [2] Kistler, A.L., "Fluctuating Wall Pressure Under Separated Supersonic Flow", *Journal of Acoustical Society of America*, Vol. 36, March 1964, pp. 543–550.
- [3] Hadjadj, A., Dussauge, J.P. "Shock wave boundary layer interaction" *Shock Waves*, Vol. 19, pp. 449–452, 2009.
- [4] Dolling, D.S. and Murphy, M.T., "Unsteadiness of the Separation Shock Wave Structure in a Supersonic Compression Ramp Flowfield," *AIAA Journal*, Vol. 21, No. 12, 1983, pp. 1628–1634.
- [5] Muck, K.C., Andreopoulos, J., and Dussauge, J.P., "Unsteady Nature of Shock-Wave/Boundary-Layer Interactions," *AIAA Journal*, Vol. 26, No. 2, 1988, pp. 179–187.
- [6] Dolling, D.S and Brusniak, L., "Separation Shock Motion in Fin, Cylinder, and Compression Ramp-Induced Turbulent Interactions," *AIAA Journal*, Vol. 27, No.6, 1989, pp. 734–742.
- [7] Blinde, P.L., Humble, R.A., Oudheusden, B.W. and Scarano, F., "Effects of Micro-Ramps on a Shock Wave/Turbulent Boundary Layer Interaction", *Shock Waves*, Vol. 19, pp. 507–520, 2009.
- [8] Babinsky, H., Makinson, N.J. and Morgan, N.J., "Micro-vortex Generator Flow Control for Supersonic Engine Inlets", *AIAA Paper 2007–0521*.
- [9] Szwaba, R., "Shock Wave Induced Separation Control by Streamwise Vortices", *Journal of Thermal Science*, Vol. 14, No. 3, 2005, pp. 249–253.
- [10] Souverein, L.J. and Debiève, J. -F, "Effect of Air Jet Vortex Generators on a shock wave Boundary Layer Interaction," *Experiments in Fluids*, Vol. 49, 2010, pp. 1053–1064.
- [11] Delery, J.M., "A Physical Introduction to Control Techniques Applied to Turbulent Separated Flows", *AIAA-2000-2606*.
- [12] Barter, J.W., Dolling, D.S., "Reduction of Fluctuating Pressure Loads in Shock/Boundary-Layer Interactions Using Vortex Generators", *AIAA Journal*, Vo. 33, No. 10, 1995, pp. 1842–1849.
- [13] Verma, S. B., Manisankar, C. and Raju, C., "Control of shock unsteadiness in shock boundary-layer interaction on a compression corner using mechanical vortex generators", *Shock Waves*, DOI 10.1007/s00193-012-0369-8.
- [14] Raju, C. and Vishwanath, P.R., "Pressure-Sensitive Paint Measurements in a Blow-down Wind Tunnel", *Journal of Aircraft*, Vol. 42, No. 4, July–Aug. 2005.

- [15] Van Driest, E.R., “Turbulent Boundary Layer in Compressible Flows,” *Journal of Aeronautical Sciences*, Vol. 18, No. 3, 1951, pp. 145.
- [16] O’Donnell R.M., “Experimental Investigation at a Mach number of 2.41 of Average Skin-Friction Coefficients and Velocity Profiles for Laminar and Turbulent Boundary Layers and an Assesment of Probe Effects”, NACA TN 3122, Jan 1954.
- [17] Verma, S.B. and Gupta, V., “Supersonic Separation with Obstructions”, *AIAA Journal*, 1996, Vol. 34, No. 4, pp. 849–850, DOI: 10.2514/3.13151.
- [18] Lin, C.C., *Turbulent Flows and Heat Transfer*, 1959.

